Electron Attachment in Gaseous Detectors

by

Rafael Dinner

Submitted to the Department of Physics
in partial fulfillment of the requirements for the degree of

Bachelor of Science in Physics

at the

MASSACHUSETTS INSTITUTE OF TECHNOLOGY

June 2000

Author .....
Department of Physics
May 5, 2000

Certified by .....
Ulrich J. Becker
Professor, Department of Physics
Thesis Supervisor

Accepted by .....
David E. Pritchard
Senior Thesis Coordinator, Department of Physics

Electron Attachment in Gaseous Detectors

by

Rafael Dinner

Submitted to the Department of Physics
on May 5, 2000, in partial fulfillment of the
requirements for the degree of
Bachelor of Science in Physics

Abstract

A drift chamber is used to measure signal strength reduction due to attachment of electrons as they drift through gas. Argon with various proportions of nitrogen, carbon dioxide, and oxygen are used. Attachment per unit drift time is found to be proportional to oxygen concentration. Linear estimates are fit to the dependence of attachment on carbon dioxide concentration. Nitrogen, while causing negligible attachment by itself, increases attachment in mixtures that are more than 10% carbon dioxide.

Thesis Supervisor: Ulrich J. Becker
Title: Professor, Department of Physics

Acknowledgments

Jesse J. Kirchner maintained and repaired the drift chamber with technical assistance from Michael Grossman. Krzysztof J. Fidkowski assisted in several measurements. Prof Becker guided the project from start to finish.

Contents

List of Figures

List of Tables

Chapter 1

Introduction

Drift chambers are the most common type of high energy physics detector. Choosing a gas mixture for use in a drift chamber and operating the chamber successfully require an understanding of the underlying process of electron drift through the gas. [1] This thesis examines attachment; that is, loss of signal due to the formation of negatively charged molecules by absorption of drifting electrons. Quantitative measurements of attachment in different gas mixtures are presented and summarized to allow estimation of attachment levels in proposed detectors.

To clarify attachment's role in chamber performance, I will summarize the processes that make up a drift chamber. When a charged particle passes through the gas in a detector, it ionizes a track of electrons. Energy loss per length traveled is given by the Bethe-Bloch formula [2],

$$\frac{dE}{dx} = \frac{4\pi NZe^4}{mc^2\beta^2} z^2 (\ln \frac{2mc^2\beta^2}{(1-\beta^2)I} - \beta^2), \tag{1.1}$$

where N is the numeric density of the gas molecules, Z is their atomic number, e is the charge of an electron, mc^2 is the rest energy of an electron, β is the particle's velocity in terms of the speed of light, z is the particle's charge in terms of e, and I is the mean excitation energy of the gas molecules. For a given gas, the number of electrons freed per length is proportional to this energy loss. These electrons drift under the influence of an applied electric field to a detection region of the chamber. There, a large electric

field near the surface of each of a few thin signal wires gives electrons enough energy over their mean free paths to ionize more gas molecules, resulting in an avalanche of electrons that is collected as a negative pulse on the wire. [3] Concurrently, a negative image charge is induced on the wire by the surrounding positive ions. The electronics primarily measure the negative image charge pulse [4], [3].

The original particle's track is then reconstructed according to $x = v_{drift}t$ from the time between its passing through the chamber (known, for example, from the collision time of the beam that generated the particle, or from some other detector such as a fast scintillator counter) and the times at which pulses are detected on signal wires. This reconstruction requires that one know the electrons' drift speed and direction. In a constant electric field applied by the chamber, the effects of many collisions average to yield a constant drift speed. The chamber can also be placed in a uniform magnetic field that produces curvature in the original particle's path, allowing calculation of momentum. If there is a component of magnetic field perpendicular to the electric field, the electrons deflect to an average angle relative to the electric field. Drift velocity and angle are important criteria for choosing a mixture. Our chamber (Fig. 2-1) is designed to measure them as a function of gas mixture composition, and electric and magnetic field strengths.

Attachment is a side-effect of the drift process. It must be controlled in order to preserve significant signals over noise. In past experiments, attachment has dramatically affected the performance of Time Projection Chambers (TPCs), which have long drift distances, and Time Expansion Chambers (TECs) [5], which have long drift times of several microseconds, causing a large amount of attachment.

A previous study [6] showed that adding controlled quantities of nitrogen to mixtures can improve drift velocity characteristics, particularly by making the chamber less sensitive to air contamination. The study concluded by examining a mixture that combined nitrogen with several common drift gases: Ar:C_2H_6:N_2:CO_2 86:5:5:4. The mixture had desirable drift velocity and angle characteristics, but appeared to attenuate signals at longer drift distances.

This thesis pursues that observation by examining the effect of nitrogen and carbon

dioxide on attachment in an argon-based mixture. I have modified the chamber electronics to measure signal strength as a function of drift distance, from which I can calculate attachment rates and their dependence on mixture composition and applied electric field. Measurements indicate that in the presence of oxygen contamination, the rate of attachment increases with the concentration of carbon dioxide, and that nitrogen enhances this effect for some mixtures. Thus chamber designers must be wary of attachment when using these otherwise desirable drift gas additives.

Chapter 2

Apparatus and methods

The drift chamber (Fig. 2-1) is described on our web page [1] and in [7]. A pulsed UV laser beam (Fig. 2-2) ionizes a track of gas molecules, simulating a high energy particle. Moving a mirror mounted on a micrometer screw allows one to change the track's position along the x-direction. A uniform electric field, $E\hat{x}$, is applied by a parallel plate arrangement between a cathode plate and an anode mesh which are separated by 2.06 cm. Electrons drift toward the grounded mesh, and a fixed proportion pass through toward five signal wires held at a high positive voltage, where they are amplified into measurable pulses. Behind the signal wires are pads DC coupled to ground. They can measure the pulses' y-coordinate via image charge to determine deflection angle in a magnetic field, but are not used in this thesis. In a "measurement," I determine signal size at different x- and E-values for one gas mixture. Smaller signal charge at longer drift distances is taken to be caused by attachment.

2.1 Ionization

The nitrogen laser produces 3.7 eV photons, so ionization is a multi-photon process, its rate per track distance varying with the area of the beam multiplied by the intensity density to a power of approximately two. So the rate increases with sharper focus. The beam is focused into the chamber by a lens with a focal length of about 100 cm

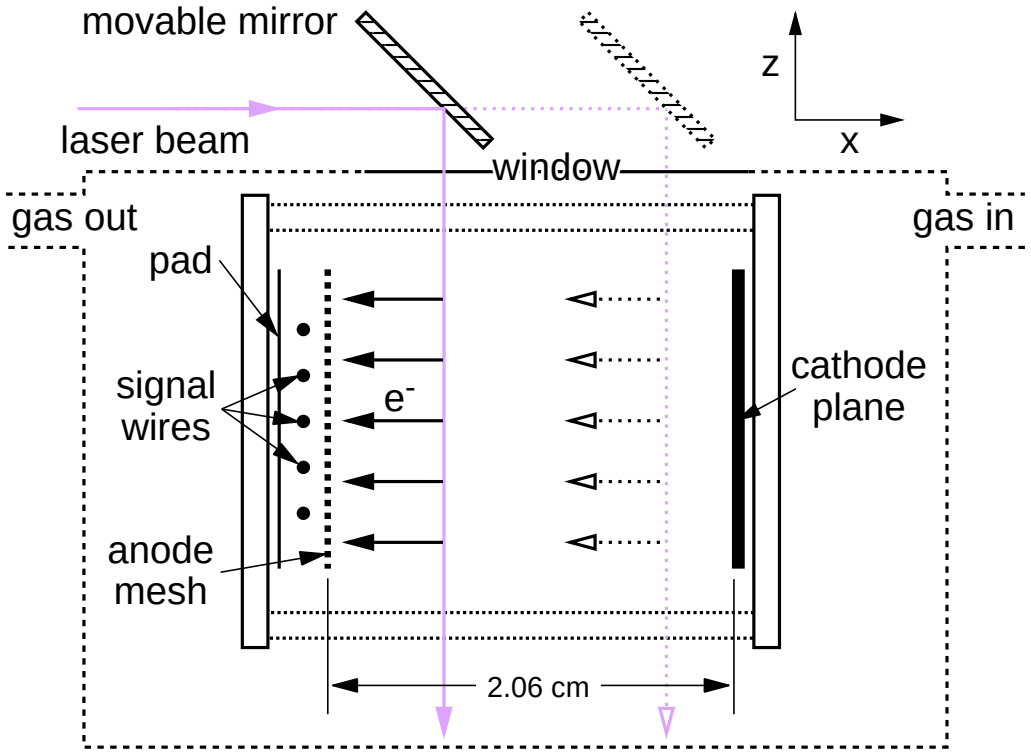

Figure 2-1: A pulsed laser beam produces a track of electron-ion pairs in the drift chamber. The beam's position is varied with a micrometer that moves a mirror.

whose position is tuned to maximize the number of electrons received by the middle signal wire in the middle of the range of laser positions. The laser is pulsed at a constant rate ($\sim$ 10 Hz) and power ($\sim$ 100 μJ) within a measurement. The pulses' lengths ($\sim$ 1–2 ns) are much shorter than electron drift times.

2.2 Gas composition

The gas is mixed from 99.998% pure components to specific proportions by adding partial pressures with a transducer. The transducer has been checked for proportionality with mechanical pressure gauges, and deviations are 0.05 PSI due primarily to fluctuations in the transducer voltage measurement. This produces an uncertainty of at most 0.2% of a mixture's total pressure, an acceptable accuracy for mixing argon, nitrogen, and carbon dioxide, which are each at least 5% of the total pressure. Small

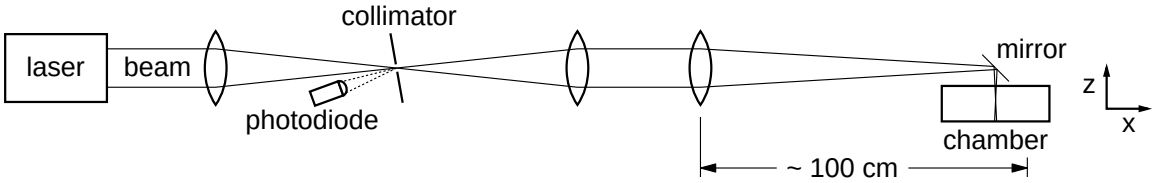

Figure 2-2: Optics focusing the laser into the chamber.

concentrations of oxygen (e.g. $0.30 \pm 0.01\%$) were achieved by diluting oxygen with argon.[1]

After equilibrating for several hours, the mixture is allowed to flow through the chamber and out to an exhaust at room pressure and temperature. A flow-controller before the chamber sets the flow to about 5 ml/s, ensuring a negligible pressure differential between the chamber and the exhaust. Due to environmental temperature and pressure fluctuation, the gas density normally changes less than 1% (rms) between measurements of different mixtures.

The gas purity is limited by the rate at which air leaks into the chamber and mixes with the gas flowing through. Several steps are taken to improve the purity of the gas used in the chamber, though. During measurements, an oil bubbler isolates the gas in the chamber from the exhaust. The chamber is also evacuated to $(5 \pm 2) \cdot 10^{-3}$ PSI prior to use (see Appendix A). Finally, when gas first fills the chamber it is allowed to flush through (at about 20 ml/s) for a minute. The flow rate is then moderated to 5 ml/s for the remainder of the measurement (approximately 20 minutes).

The *leak rate* is the rate at which air outside the chamber at one atmosphere leaks into the chamber. It was determined by evacuating the chamber and sealing it off. Pressure in the chamber rose by 0.5 PSI per hour.

This leak rate combines with the flow rate during a measurement. I assume the

[1]For example, the mixture Ar:N_2:CO_2:O_2 balance:5:10:0.3 is made by diluting 1.8 PSI of oxygen to 45 PSI with argon, vacuuming part of the mixture to leave 1.8 PSI, adding 1.2 PSI of nitrogen, adding 2.4 PSI of carbon dioxide, then adding argon to a final pressure of 24.0 PSI:

$$\frac{1.80 \pm 0.05}{45.00 \pm 0.05} \cdot \frac{1.80 \pm 0.05}{24.00 \pm 0.05} = (0.30 \pm 0.01)\%. \tag{2.1}$$

air leaking in mixes evenly with the chamber's contents and that this homogeneous mixture is what flows out at 5 ml/s. The volume of the chamber and associated piping is about 2000 ml, so the flow rate f is

$$f = \frac{5\,\mathrm{ml/s} \cdot 3600\,\mathrm{s/hr}}{2000\ ml} = 9.0\,\mathrm{chamber\ volumes\ per\ hour}. \tag{2.2}$$

The partial pressure, p, of air in the chamber multiplied by f is the rate at which air contamination is removed by the flow. The rate at which p changes is then equal to the rate at which air leaks in minus the rate at which the air flows out:

$$\frac{dp}{dt} = leak\,rate - f \cdot p. \tag{2.3}$$

The solution of this equation is

$$p(t) = (p_0 - p_f)e^{-ft} + p_f \tag{2.4}$$

where p_0 is initial pressure and p_f is pressure at $t = \infty$ (at which $dp/dt = 0$):

$$p_f = \frac{leak\,rate}{f} = \frac{0.5\,\mathrm{PSI/hr}}{9.0\,\mathrm{volumes/hr}} = 5.6 \cdot 10^{-2}\,\mathrm{PSI}. \tag{2.5}$$

Atmospheric pressure is 14.7 PSI, so the equilibrium air contamination is

$$\frac{5.6 \cdot 10^{-2}\,\mathrm{PSI}}{14.7\,\mathrm{PSI}} = 3800\,\mathrm{PPM}. \tag{2.6}$$

Oxygen is 20.9%, or 790 PPM, of the total contamination. The oxygen rises to this level with a time constant of $1/f = 0.11$ hours $= 7$ minutes. To account for this upper bound on contamination, the calculated oxygen levels were increased by 400 PPM and their uncertainties were widened to ± 400 PPM.

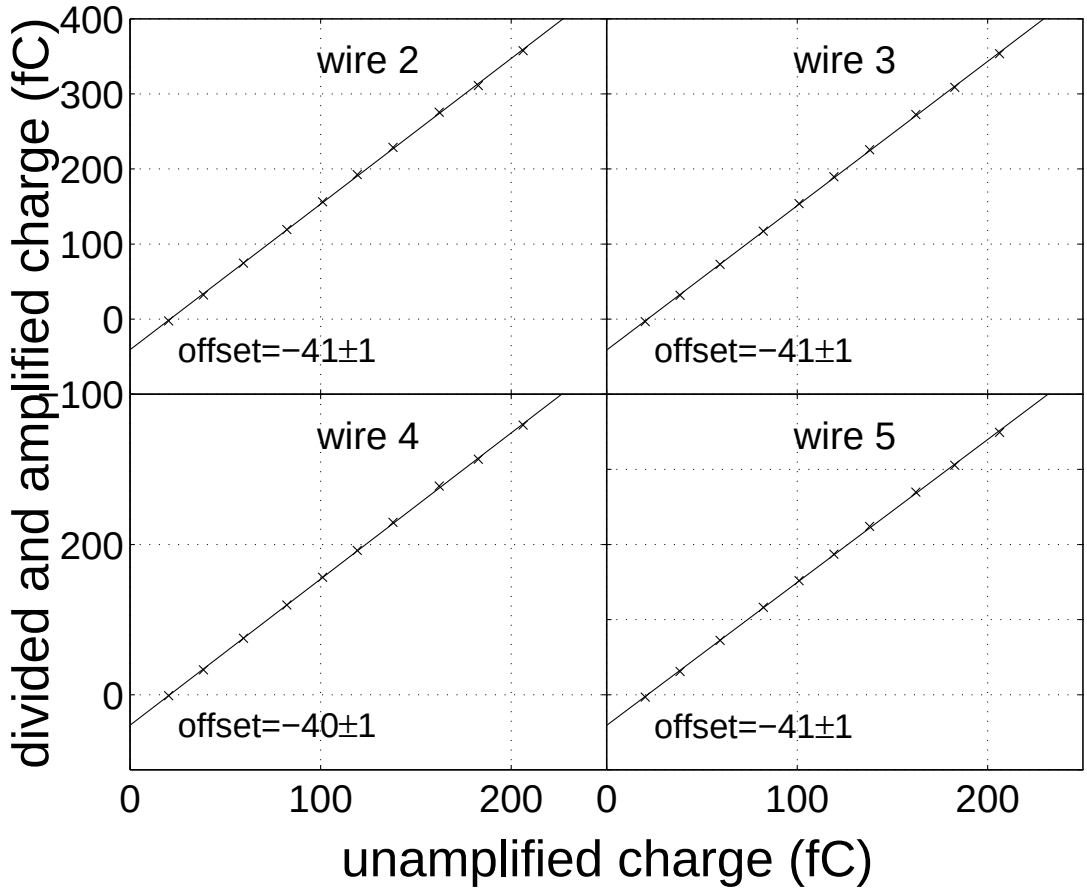

Figure 2-3: The signal wire amplifiers produce negative offsets in measured charge, which were subtracted to obtain measurements proportional to unamplified charge.

2.3 Pulse measurement

The signal wires are 25 μm in diameter and typically held at about 1200 V, which puts them in the "proportional" gain region of voltage: The number of electrons deposited on the signal wires (and therefore the charges of the image pulses) is proportional by some gain factor to the number of electrons that pass through the mesh into the amplification region of the chamber. Each wire's pulse's charge is then amplified electronically by a factor of about 1000. Charge integrating ADCs measure the amplified signal.

The amplifiers were calibrated (Fig. 2-3) using square pulses from a pulse generator. The pulses were attenuated to ten different levels. At each level, they were first

measured directly by the charge-integrating ADCs, which have a 50 Ω load. They were then resistively divided and applied to the amplifiers as shown in Fig. 2-4. The high resistances in series with the amplifiers simulated signal wires, which approximate current sources. For both the amplified and unamplified pulses, and for experimental data, ADC pedestals (with quiescent input signals) are first measured, then subtracted from subsequent measurements. In addition to subtracting these pedestals, it was determined that offsets of about 41 fC must be added to the measured charges to achieve proportionality between unamplified and amplified pulses.

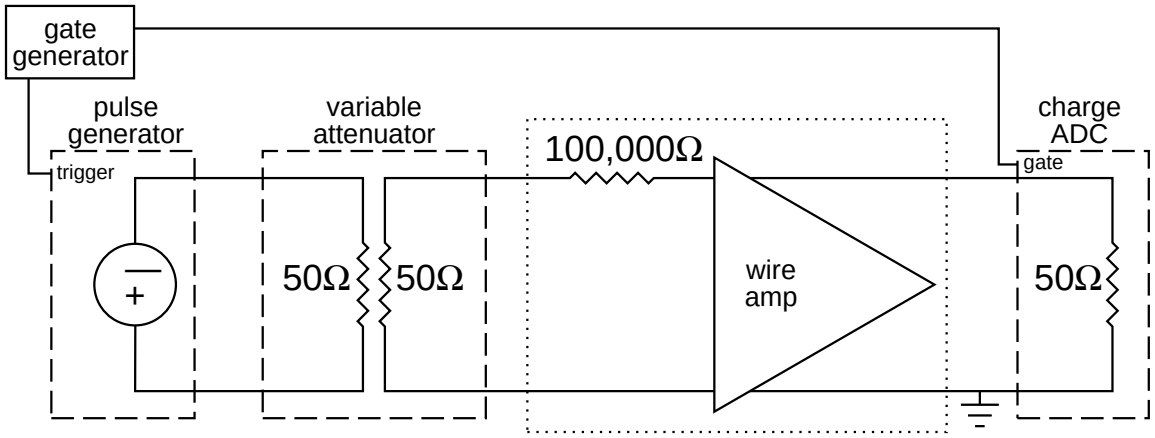

Figure 2-4: To calibrate each amp, square pulses were attenuated to various voltages, then measured. They were measured without amplification by removing the series resistance and the amplifier, shown in the dotted box. They were then measured with these components.

Amplified pulses are gated for charge integrating ADC measurement by a coincidence between the laser firing and a discriminator measuring an appreciable pulse on signal wire 1, which is designated as a trigger for gating the pulses on wires 2–5 (Fig. 2-5). Wires 2–5's pulses are passed through 200 ns delays to four ADCs' analog inputs. Electrons drift across the 2.06 cm long chamber at roughly 1 cm/μs, so they arrive at the signal wires a couple of microseconds after the laser fires. The gate from the laser is therefore chosen to be 10 μs. It is triggered by a photodiode that receives laser light reflected from the collimator. Each measurement is repeated for about 100 laser shots such that the standard deviation of the mean charge is less

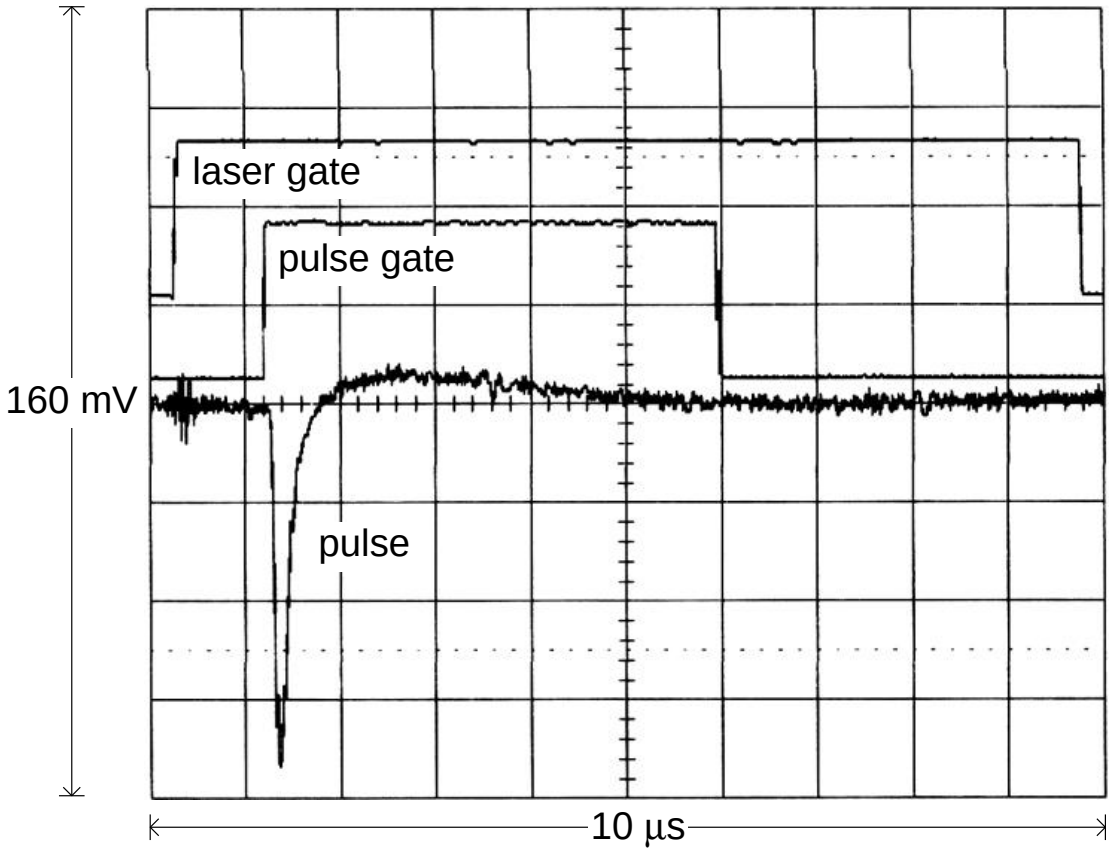

Figure 2-5: An amplified pulse from signal wire 5 is gated by a coincidence between the laser firing and detection of a pulse on signal wire 1, used as a trigger. The positive over-swing is due to AC coupling and does not affect relative measurements.

than 1%. A histogram of several hundred shots (Fig. 2-6) with 20-channel-wide bins shows that the mean is well defined by a narrow distribution. The mean charge and its uncertainty are recorded by a computer.

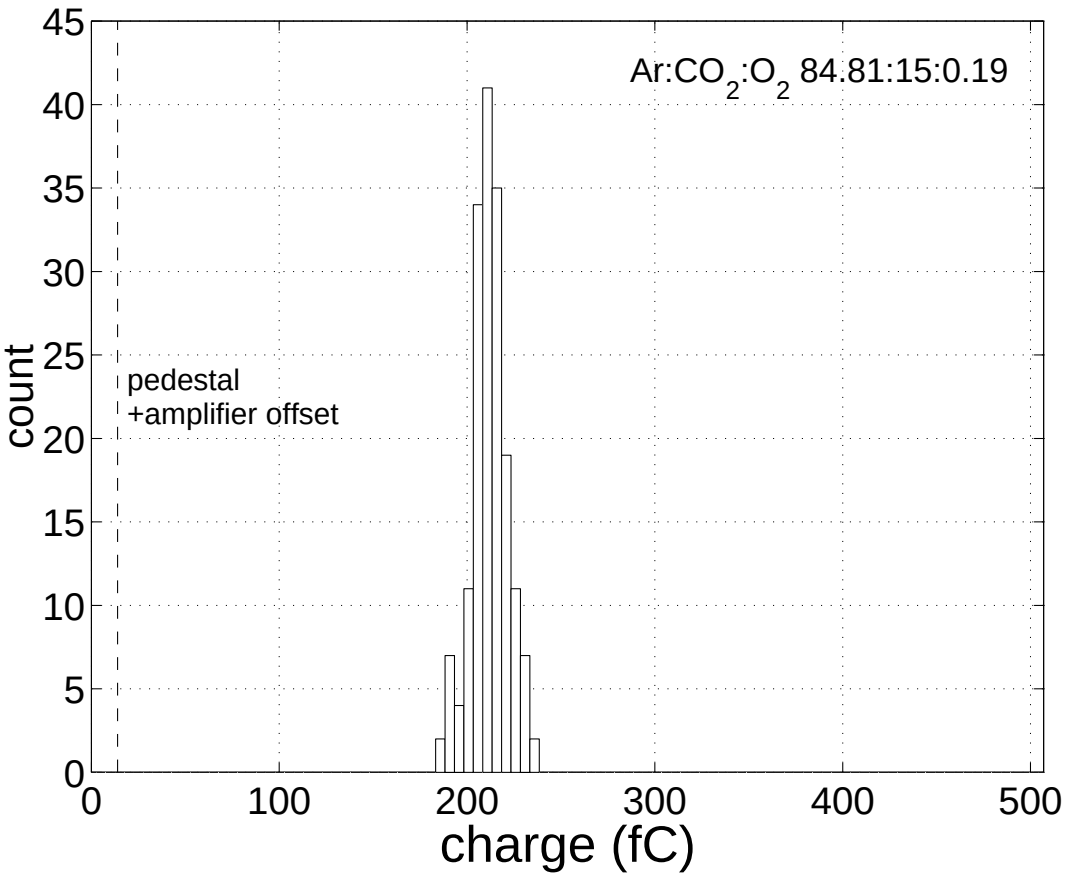

Figure 2-6: A histogram of repeated measurements of charge allows calculation of a mean signal size and its uncertainty.

2.4 Software for control and data acquisition

I created PC software to automate many aspects of the experiment, including instrument control and data acquisition (DAQ). I used LabVIEW development software [2] to package these capabilities in a graphical interface. Fig. 2-7 shows the highest-level control interface. This software sets the electric field in the chamber via a digital-to-analog board[3] attached to a high voltage supply. It then runs the DAQ routine

[2]National Instruments' LabVIEW 5.0 compiles code written in its graphical programming language, "G," and includes routines for using data acquisition hardware, analyzing data, and creating graphical interfaces.

[3]National Instruments' PC-AO-2DC board provides a voltage source controlled by a 12-bit DAC. With my chamber setup, this voltage resolution translates to setting the electric field in increments of 1.185 V/cm.

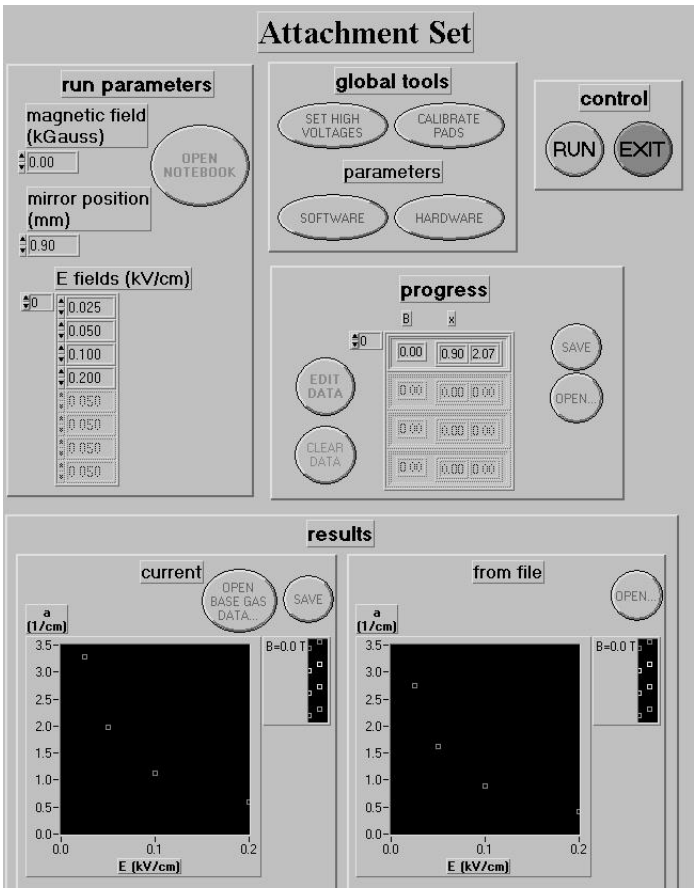

Figure 2-7: A graphical interface written for the experiment controls the data acquisition process and calculates attachment levels for output to log files.

shown in Fig. 2-8.

This routine reads out ADC measurements from a CAMAC instrumentation crate with a GPIB-to-CAMAC controller and a GPIB interface board, controlled by LabVIEW drivers. It waits for the CAMAC crate to signal that the instrumentation has received data, which occurs when a coincident gate is received by the ADC. The routine then retrieves the ADC measurements and gives the experimenter immediate feedback: It displays the distribution of charges on the different signal wires and histograms the charge distribution from previous events. After displaying an event, the routine resumes waiting, and repeats this procedure until it has collected 100 events (from 100 laser pulses). The data is then averaged and passed back to the control routine.

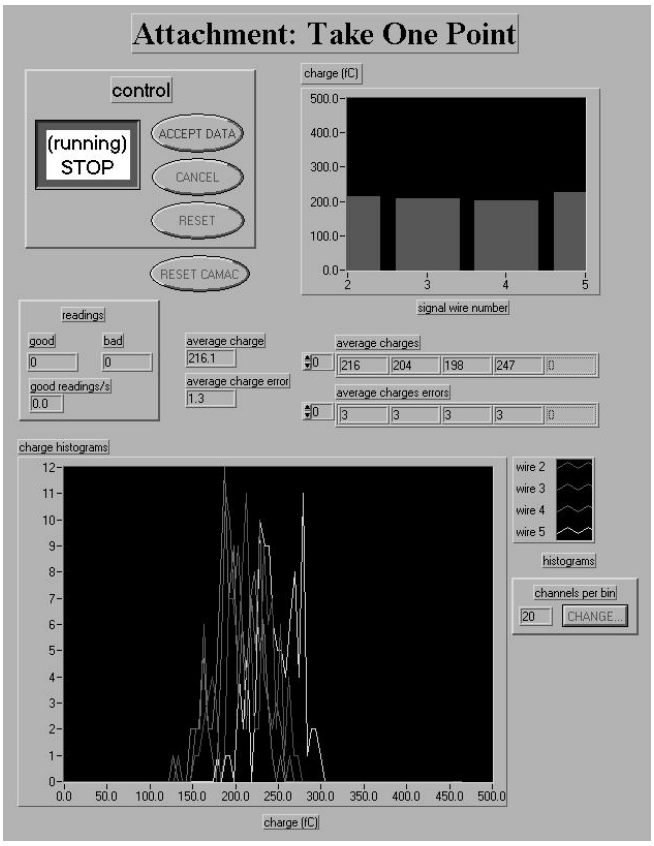

Figure 2-8: The routine that records instrument data and provides immediate graphical feedback.

The control software iterates through different electric fields, then allows the experimenter to move the mirror to a new x. It also allows one to apply different magnetic fields to the chamber and record separate data sets for each field, although magnetic fields were not used in these measurements. After collecting data from different mirror positions at each electric and magnetic field, the software calculates and displays the corresponding attachment level. These results are graphed ans written to a log file for further analysis.

2.5 Drift velocity measurement

I wrote similar control and data acquisition software for measuring electron drift velocity. Empirical drift velocity measurements were used to check simulations (see

Section 2.9). Velocities were measured with the same chamber; in fact, the chamber was designed to measure drift velocity and Lorentz deflection angle as described in [7]. At each of two mirror positions, x_1 and x_2, relative drift times are measured between the laser triggering the photodiode and a signal wire triggering its discriminator. Drift velocity is calculated from the differential values,

$$v_{drift} = \frac{\Delta x}{\Delta t} = \frac{x_1 - x_2}{t_1 - t_2}. \tag{2.7}$$

The differential calculation cancels offsets in time (signal delays) and drift length. For the mixtures and electric fields used, the drift times were too long for the CAMAC-based time-to-digital converter to measure, so they were measured with a digital oscilloscope. The velocities have an estimated uncertainty of 1% when comparing different mixtures [7].

2.6 Attachment calibration

To determine signal strength as a function of drift length, x, two sets of signal charge measurements were used. Signal size at different mirror positions, x, is first measured in a calibration gas at one electric field, where attachment is known to be negligible (see Section 2.8). The wires' measurements are averaged to obtain $Q_1(x)$. Signal size in the attaching mixture, $Q_2(x)$, is then measured for each wire at the same set of mirror positions, and several electric field strengths at each position. S is the normalized signal size $Q_2(x)/Q_1(x)$. This calibration eliminates non-uniformities caused by factors that persist between the two data sets, such as a non-uniform number of primary electrons with changing mirror position due to a change in the focus of the laser beam.

2.7 Analysis procedure

Drifting electrons have an average energy of at least thermal energy, $kT = 1/40$ eV, which corresponds to a velocity of 9.4 cm/μs.[4] Drift velocities are an order of magnitude smaller than this.[5] Drift falls into an equilibrium between the effects of an electric field and collisions. The drift distance dx in a time interval dt reaches an equilibrium, leading to a constant drift velocity in a uniform electric field.

One expects a similar picture for attachment: In a given time interval dt, collisions at a distribution of energies occur, averaging to a constant probability that an electron is absorbed. In this case, a constant fraction of the electrons, and ultimately the signal size, S, is absorbed:

$$\frac{dS}{dt} = -\beta S, \tag{2.8}$$

so S will be an exponential function of drift time, t:

$$S = S_0 e^{-\beta t}. \tag{2.9}$$

Furthermore, for a constant drift velocity, $t = x/v_{drift}$ and

$$S = S_0 e^{-ax}. \tag{2.10}$$

where

$$a = \beta / v_{drift}. \tag{2.11}$$

The attachment rate, a, is a positive number with units of inverse length. Equation 2.10 represents the data well, as indicated by an example shown in Fig. 2-9. The data is fit with an exponential to find a single value of a from numerous measurements of $S(x)$. The inverse of a gives a characteristic length for the signal decay.

S versus x for each of wires 2–5 at each electric field is fit to an exponential,

[4] Dropping across an electric potential will increase the electrons' energies and inelastic collisions with gas molecules will decrease their energies, leading to an equilibrium over many collisions. A simulation by Magboltz (see Section 2.9) of electrons drifting in Ar:N_2:CO_2:O_2 84.85:5:10:0.15 with an electric field of 0.1 kV/cm predicts an average electron energy of 0.0404 eV, or 11.9 cm/μs.

[5] For the mixture described above, Magboltz predicts a drift velocity of 0.602 cm/μs.

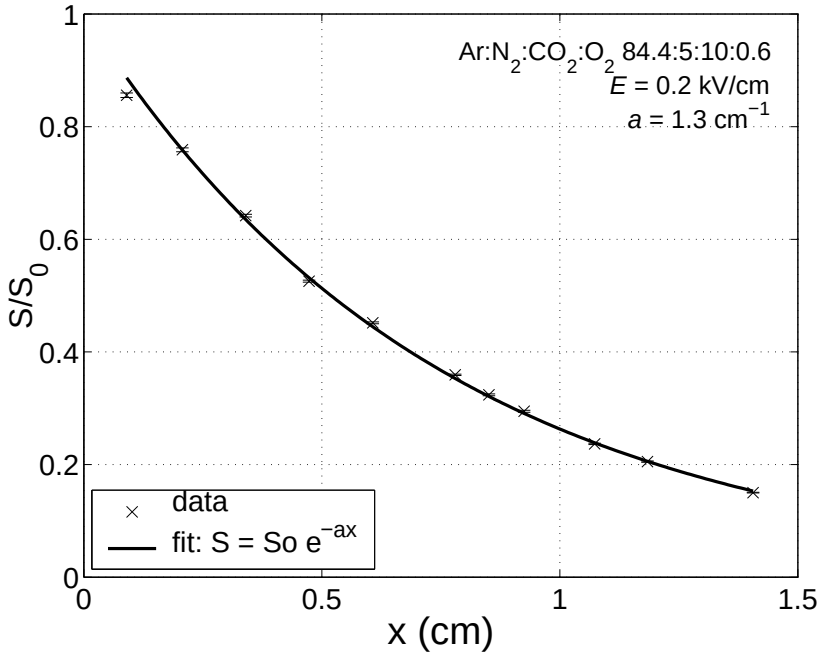

Figure 2-9: Measured signal size in an attaching gas mixture obeys $S = S_0 e^{-ax}$, where x is drift distance.

yielding a value of a. Finally, a is calculated for each electric field as the mean of the a-values for the individual wires' data.

2.8 Error estimates

Because attachment represents the decay constant of an exponential, it is independent of the amplitude of the exponential. This is fortunate, because the amplitude is very sensitive to factors such gas density, signal wire voltage, and laser intensity, all of which may vary between measurements. Any shift in the absolute values of measured drift lengths would also change the amplitude while leaving attachment unaffected.

So the systematic error is confined to only those factors that affect S $(= Q_1/Q_2)$ by transforming it nonlinearly, or affect it unequally at different mirror positions. For example, if the temperature rose significantly over the course of a measurement, the density of the gas would decrease. This is known to affect the signal wires' gain by increasing the mean free path between collisions, which allows the electrons to

accelerate to higher energies at which their collisions are more likely to be ionizing. Thus gain would increase with time; that is, measurements at later times would include more gas amplification. The x positions were always taken in ascending order, so this would increase signal size at longer drift distances, decreasing the attachment calculated.

Ar:CH_4 90:10 ("P10") was used for calibration, and was repeatedly measured between every few data sets. One can see that attachment is negligible in this mixture from three considerations. First, by assuming that non-uniformities such as the focusing effect described above are small, and fitting the unnormalized charges with exponentials, one discovers that any exponential factor is within statistical fluctuations of zero: the mean is 0.01 ± 0.03 1/cm. Second, P10 displays approximately the same profile of Q versus x as another gas supposed to have negligible attachment, Ar:C_2H_6 50:50 (Fig. 2-10). If either mixture attached, it is unlikely that the two

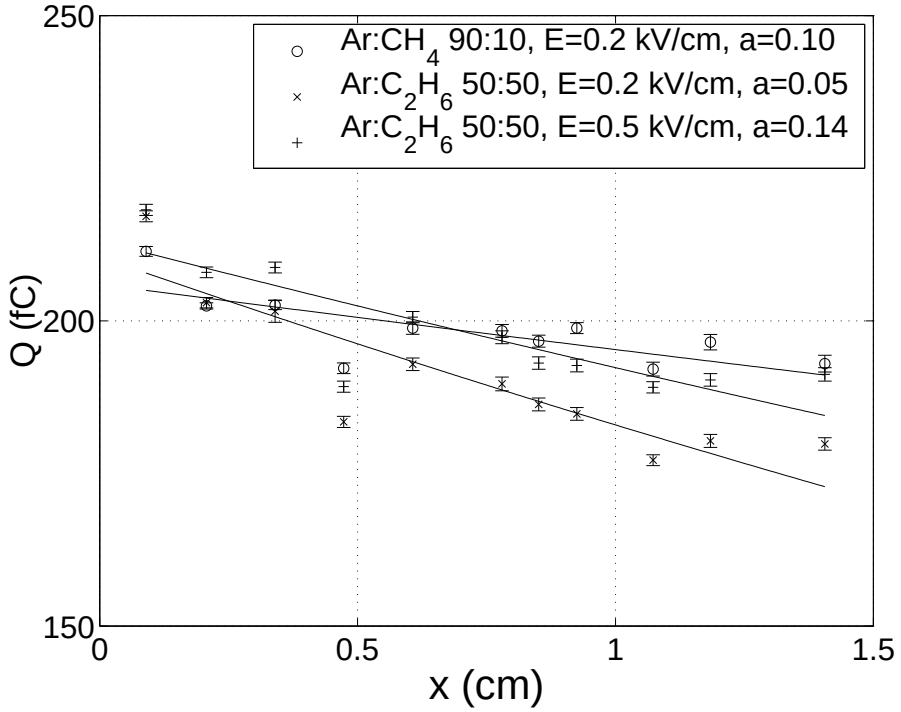

Figure 2-10: Signal size variation with drift distance does not deviate between Ar:C_2H_6 50:50 and P10 more than the fluctuations of 0.07 cm^{-1} between P10 measurements, indicating that neither mixture attaches significantly.

	E (kV/cm)			
	0.025	0.050	0.100	0.200
day 1: a (1/cm)	–	2.11±0.03	1.301±0.005	0.719±0.003
day 2: a (1/cm)	3.00±0.04	2.12±0.02	1.259±0.004	0.660±0.004
day 3: a (1/cm)	3.45±0.07	2.06±0.01	1.279±0.004	0.717±0.005
day 4: a (1/cm)	3.25±0.03	1.94±0.01	1.130±0.004	0.602±0.008
mean	3.2	2.06	1.24	0.67
day-to-day fluctuation	0.2	0.08	0.08	0.06

Table 2.1: Repeatability of attachment measurements. The uncertainties on individual values are obtained from statistical fluctuation between events within one measurement. They are insignificant compared to the fluctuations between measurements.

would agree. Finally, a simulation by Magboltz predicts no attachment in P10.[6]

The effect on calculated attachment of a non-uniformity in calibration data is also best expressed by fitting an exponential to the calibration data, because if the deviation has an exponential component, δ, it will directly subtract from a:

$$\frac{Q_1 e^{-ax}}{Q_2 e^{-\delta x}} = \frac{Q_1}{Q_2} e^{-(a-\delta)x}. \tag{2.12}$$

The fluctuation in the exponential coefficients of the calibrations data (0.07 1/cm) therefore provides an estimate of the uncertainty calibrations introduce into the values of attachment calculated using those calibrations.

Because it was suspected that systematic fluctuations between measurements dwarfed the statistical error estimates obtained by iteration within a measurement, an attaching mixture, Ar:N_2:CO_2:O_2 balance:5:10:0.3 was chosen and measured on several different days (but compared to the same calibration) (see Table 2.1). The standard deviation of the a-values indicates that the uncertainty of a is approximately proportional to a (6% of a) and an order of magnitude larger than the uncertainty predicted by iteration within measurements. Combining this with the uncertainty between calibrations of 0.07 cm^{-1}, successive a-values were assigned errors of the quadrature sum of 6% and 0.07 1/cm.

[6]See section 2.9 for the cross sections used.

2.9 Simulations

The Magboltz program v3.0 [8] simulates electron drift, solving the Boltzmann transport equations with a Monte-Carlo method. It takes in energy-dependent cross sections for interactions such as elastic scattering and attachment.[7] Its calculations of attachment coefficients do not agree well with the measured data. Figures 2-11, 2-12, and 2-13 compare the measured to simulated dependence of attachment on concentrations of oxygen, nitrogen, and carbon dioxide, respectively.

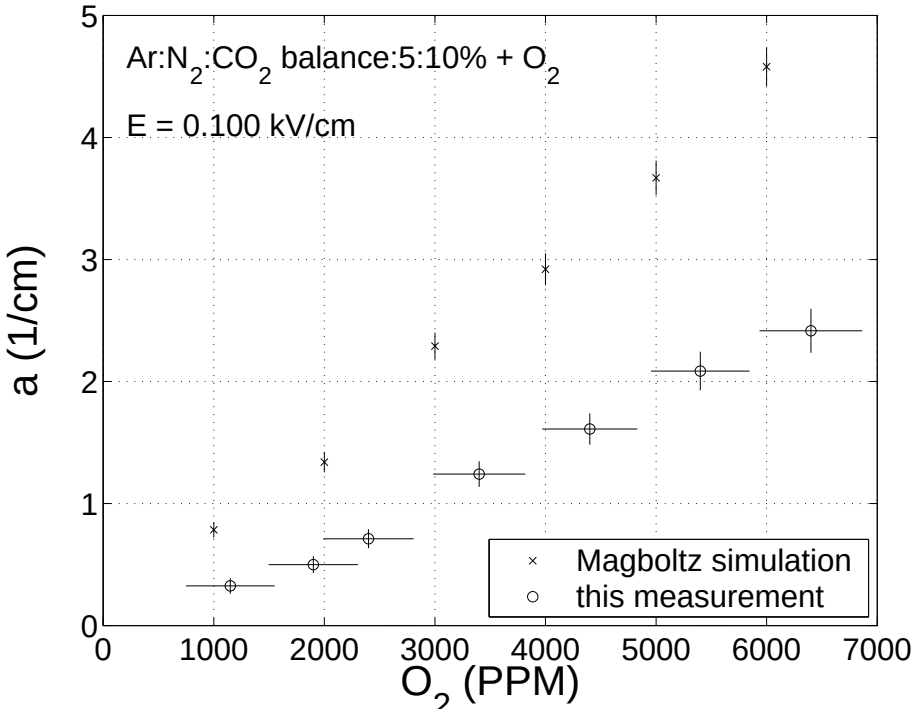

Figure 2-11: Comparison of empirical data to simulations by Magboltz for the dependence of attachment on oxygen level.

Magboltz's calculations of drift velocity, however, accord with empirical data. Simulated velocities are compared to empirical data in Fig. 2-14.

Magboltz is therefore used to simulate drift velocities. It is also used to simulate collision rates. Attachment rates, however, are taken from my empirical data.

[7] The cross sections used were distributed with Magboltz v3.0 in September, 1999. They are identified as "Argon 1997," "Methane 1994," "Nitrogen: Pitchford and Phelps, N2Mod," "CO2 1997," and "Oxygen 1990 with 3-body attachment."

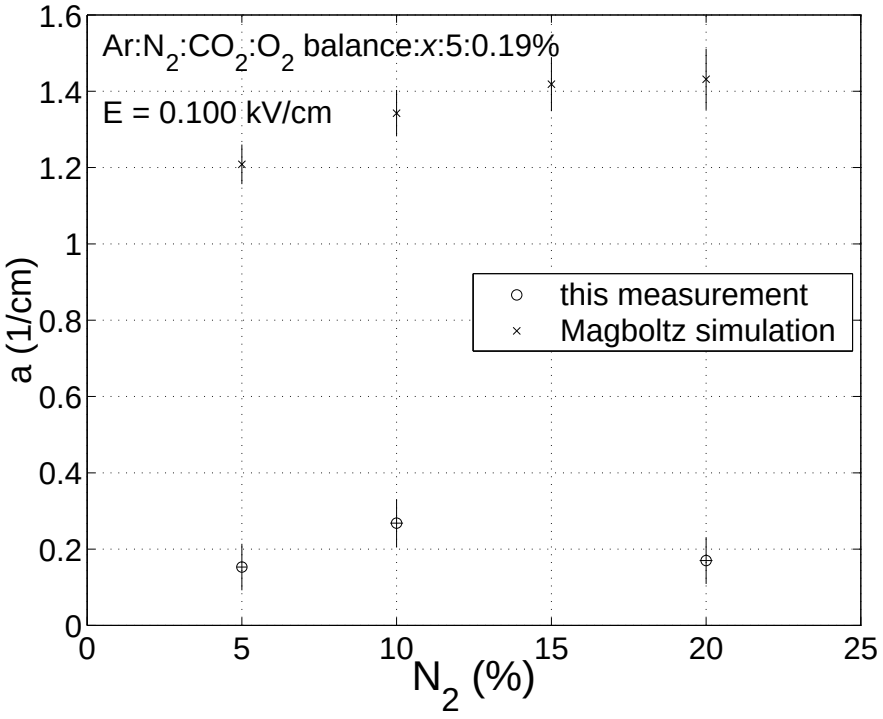

Figure 2-12: Comparison with simulations for the effect of nitrogen level.

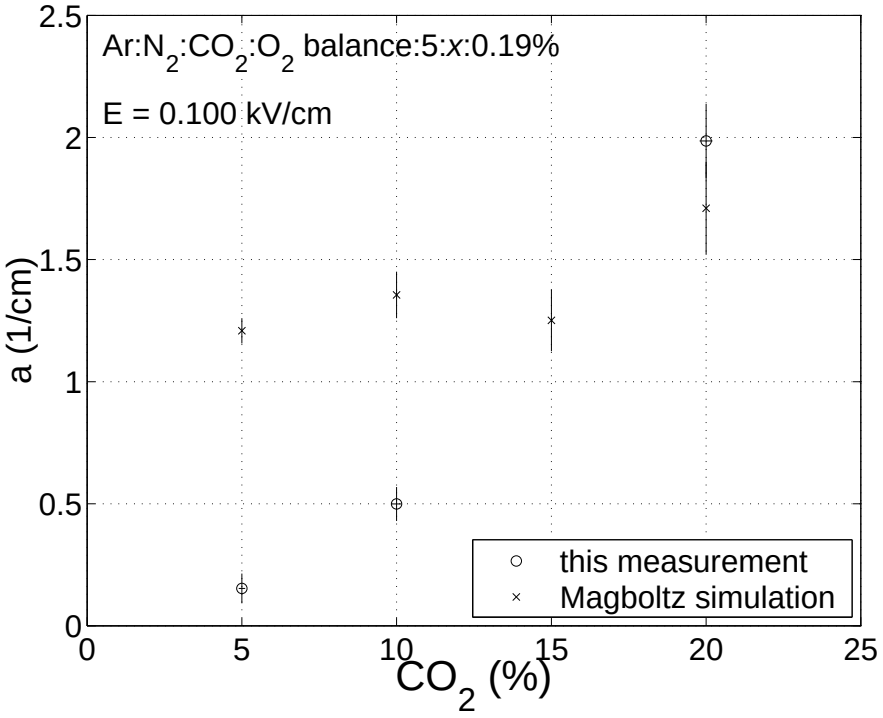

Figure 2-13: Comparison with simulations for the effect of carbon dioxide level.

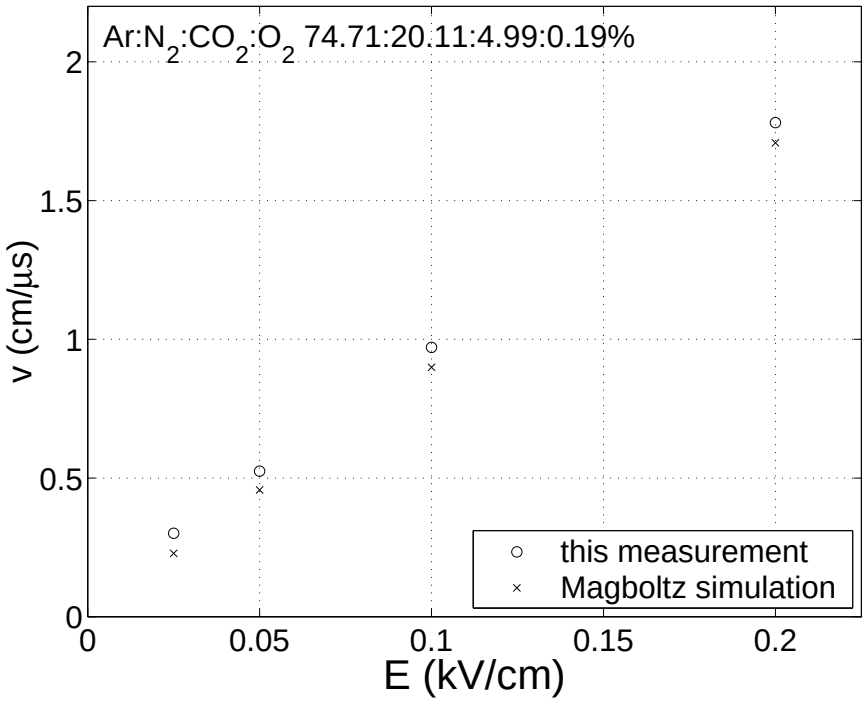

Figure 2-14: Comparison of measured to simulated drift velocities.

Chapter 3

Data and evaluation

The mixtures studied were chosen to represent potential drift gases, such as those studied in [6], with small oxygen concentrations due to unavoidable air contamination. However, in order to minimize the effects of uncertainties in the measurements, oxygen levels were set much higher than would be found in a typical drift chamber. Measurements of the exaggerated amount of attachment in these mixtures extrapolate to realistic levels by fitting attachment as a function of oxygen concentration with a simple polynomial. Similarly, polynomial fits are made for attachment as a function of carbon dioxide levels in an attempt to compactly characterize the effect of arbitrary concentrations.

Fitting the data to establish a polynomial relationship between the concentration of different components and attachment also gives insight into the underlying collision processes: Each reaction's rate is proportional to the concentration of each of the molecules required, so the power of the dependence of attachment on concentration of a gas represents the number of molecules of that gas involved in the attachment process. There may be more than one process that leads to attachment, in which case the polynomial dependence could have multiple terms.

The measured values of attachment per drift length are first analyzed for each electric field separately. The dependence on electric field is then shown to be characterized by its effect on drift velocity.

3.1 Oxygen dependence of attachment

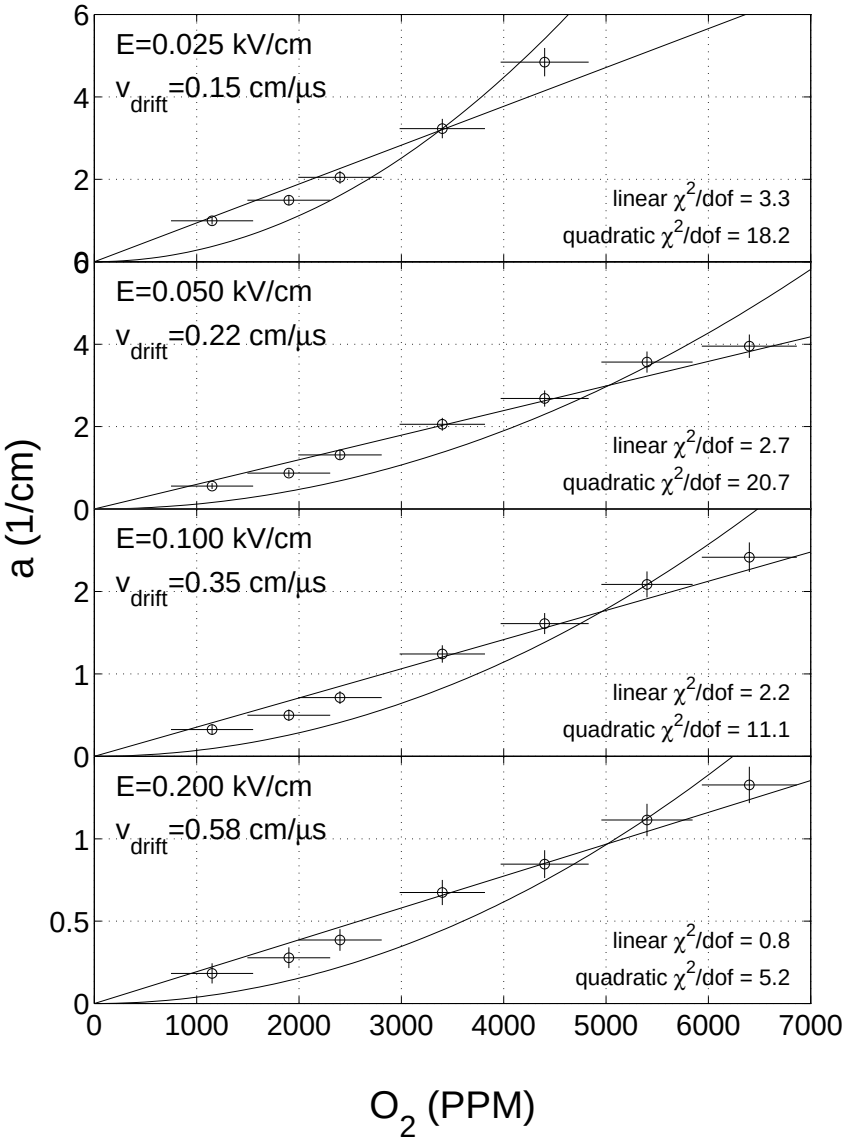

Figure 3-1: Dependence of attachment on oxygen level at several electric field strengths.

Attachment was found to be proportional to oxygen concentration to within experimental error (Fig. 3-1). This simple relationship allows extrapolation to the lower levels of oxygen normally found in drift chambers.

3.1.1 Unifying electric field data

The data from different electric fields can be expressed more compactly in terms of attachment per drift time, $\beta = av_{drift}$ (see Equation 2.11). Electric field strength affects drift velocity, but because v_{drift} only changes a small component of the electron's actual velocity (see Section 2.7), the number of collisions per unit time does not change significantly. β is not, therefore, highly dependent on electric field.

This reduction of E dependence is shown in Fig. 3-2 for the measurements of oxygen dependence in the base mixture Ar:N_2:CO_2 85:5:10. Measured values of a are normalized by simulated drift velocities (see Section 2.9) to obtain values of β. The normalization accounts for most of the disparity between the different electric

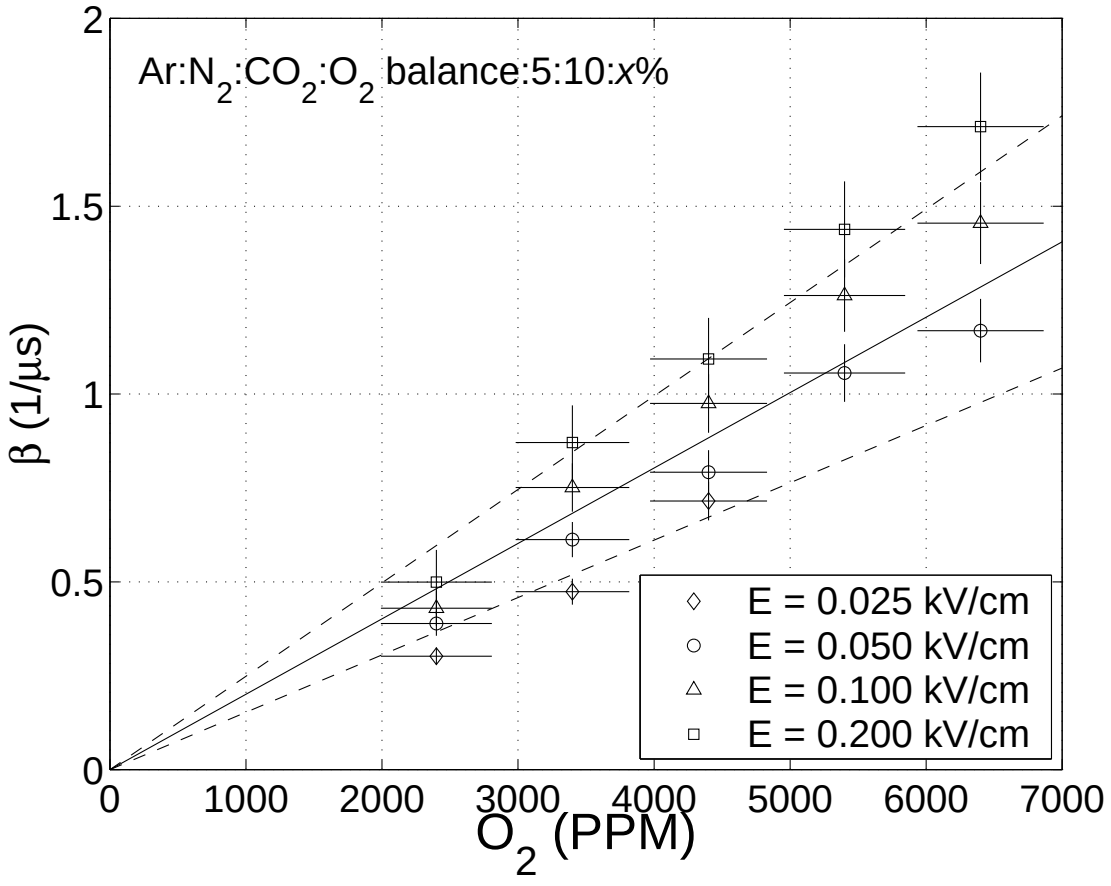

Figure 3-2: Normalizing empirical measurements by Magboltz's simulated drift velocities largely eliminates the disparity between different electric fields for the dependence of attachment on oxygen level.

fields, and fitting a single proportionality between attachment per unit drift time and oxygen concentration, one finds

$$\beta = (2.0 \pm 0.5) \cdot 10^{-4} \,\text{per microsecond per PPM } O_2 \tag{3.1}$$

Multiplying this rate constant by oxygen level, then plugging this attachment rate into Equation 2.9 yields an estimate of signal attenuation in the base mixture of Ar:N_2:CO_2 85:5:10 for electric fields in the range of 0.025–0.200 kV/cm.

3.1.2 Comparison of measured attachment to a predicted upper bound

The attachment rate is proportional to the concentration of oxygen to the first power, indicating that one molecule of O_2 is involved in the dominant attachment process. This accords with the calculations and data cited by Herzenberg [9]. Herzenberg estimated an upper bound on the rate constant, K, for the Bloch-Bradbury three-body attachment mechanism in which oxygen initially attaches the electron but must be stabilized by collision with another molecule to retain the electron:

$$e^- + O_2 + X \rightarrow O_2^{-*} + X \rightarrow O_2^- + X. \tag{3.2}$$

The rate equation is

$$\beta = K N_O N_X, \tag{3.3}$$

where N_O is the numeric density of O_2 in $1/\text{cm}^3$ and N_X is the numeric density of the stabilizing molecule X in $1/\text{cm}^3$. The upper bound for K is that it be on the order of 10^{-36} $\text{cm}^6/\mu\text{s}$ at room temperature. This translates to an upper bound on β/N_O by assuming all molecules in the Ar:N_2:CO_2:O_2 mixture can act as the stabilizer X. In this case, N_X is the numeric density of the whole mixture,

$$N_X = N = 2.7 \cdot 10^{19} \, 1/\text{cm}^3. \tag{3.4}$$

One PPM of O_2 is a concentration of $N/10^6$. So

$$\beta = KN(N/10^6) \sim 7 \cdot 10^{-4} \text{ per } \mu\text{s per PPM } O_2 \tag{3.5}$$

Equation 3.1 gave $\beta = (2.0 \pm 0.5) \cdot 10^{-4}$ per μs per PPM O_2, which satisfies the upper bound given by Equation 3.5.

3.2 Carbon dioxide dependence

First, carbon dioxide's and nitrogen's independent abilities to enhance attachment in the presence of oxygen contamination were measured.

Fig. 3-3 shows attachment with different concentrations of CO_2 normalized by simulated drift velocities. Oxygen concentration is fixed at 1900 PPM and the balance of the mixture is argon.

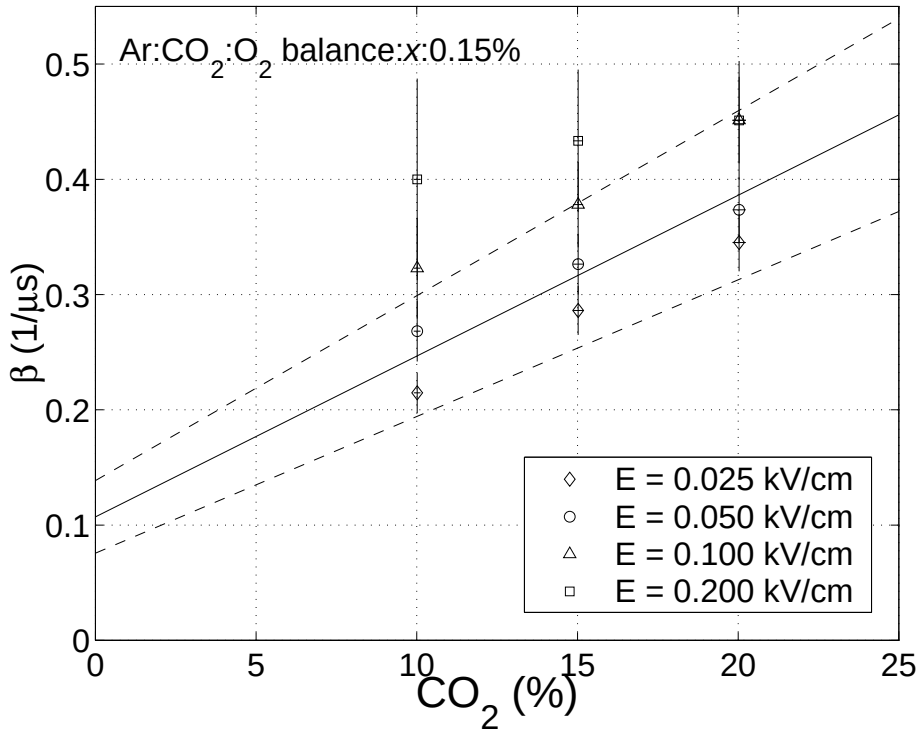

Figure 3-3: Attachment variation with carbon dioxide concentration. The solid line was fit to the data, with uncertainty represented by the dashed lines.

The data was fit to a line,

$$\beta\,(1/\mu\mathrm{s}) = (0.014 \pm 0.002)(\%\,\mathrm{CO_2}) + (0.11 \pm 0.03) \tag{3.6}$$

although the data may be consistent with other extrapolations. Assuming the attachment rate is proportional to oxygen concentration as in Section 3.1 with Ar:N_2:CO_2 85:5:10, Equation 3.6 can be restated as

$$\beta\,(1/\mu\mathrm{s}) = (((7 \pm 2) \cdot 10^{-6})(\%\,\mathrm{CO_2}) + (6 \pm 2) \cdot 10^{-5})(\mathrm{PPM\,O_2}) \tag{3.7}$$

3.2.1 Comparison to an existing CO_2 measurement

Signal attenuation due to oxygen contamination in CO_2:iC_4H_{10} 90:10 was measured by Kurihara *et al.* [10] Their paper shows data for 60 PPM and 120 PPM of O_2 (see Fig. 3-4). Their electric field is 1.42 kV/cm over a drift length of almost 5 cm.

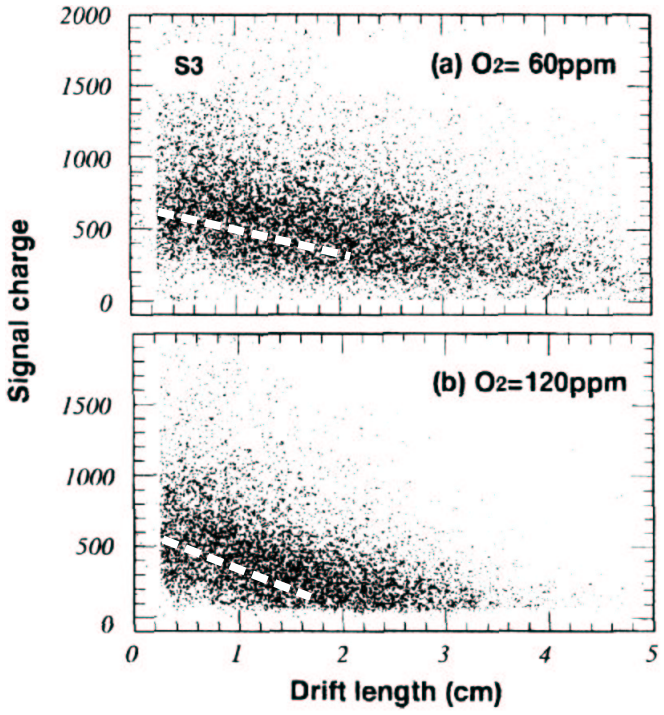

Figure 3-4: For comparison with my measurements, I used measurements of signal charge as a function of drift length (dots) in CO_2:iC_4H_{10} 90:10 published by Kurihara [10]. I estimated attachment rates for the mixture from the initial value and slope of the signal decay, indicated by the dashed lines (added).

They used a simulation with confirming measurements to determine a drift velocity, $v_{drift} = 0.71$ cm/μs. I estimated the initial value, S, and slope, dS/dx, of the signal decay for each oxygen level, then calculated $a = -(dS/dx)/S$ (see Equation 2.10) and $\beta = av_{drift}$ (see Equation 2.11). To compare, I used Equation 3.7 to extrapolate a value of β for an argon-based mixture with the same amounts of CO_2 (90%) and O_2 (60 and 120 PPM). The results are shown in Table 3.1. The mixtures are consistent to within an order of magnitude, but not within experimental error. The disparity might reflect differences between argon and isobutane, or a failure of the fits I used

O_2 PPM	Kurihara's CO_2:iC_4H_{10} 90:10 estimated a (1/cm)	β ($1/\mu$s)	my Ar:CO_2 10:90 extrapolated β ($1/\mu$s)
60	0.27	0.19	0.04±0.01
120	0.53	0.38	0.09±0.02

Table 3.1: Attachment rates estimated from Kurihara's measurements [10] of signal decay in CO_2:iC_4H_{10} 90:10 (see Fig. 3-4) are compared to extrapolated values from my measurements with Ar:CO_2 mixtures.

to extrapolate attachment's dependence on carbon dioxide concentration and proportionality to oxygen concentration. It may also be an artifact of the method I used to estimate attachment from the given signal size data.

3.3 Nitrogen's enhancement of attachment

Nitrogen without carbon dioxide does not produce significant attachment, as shown in Fig. 3-5.

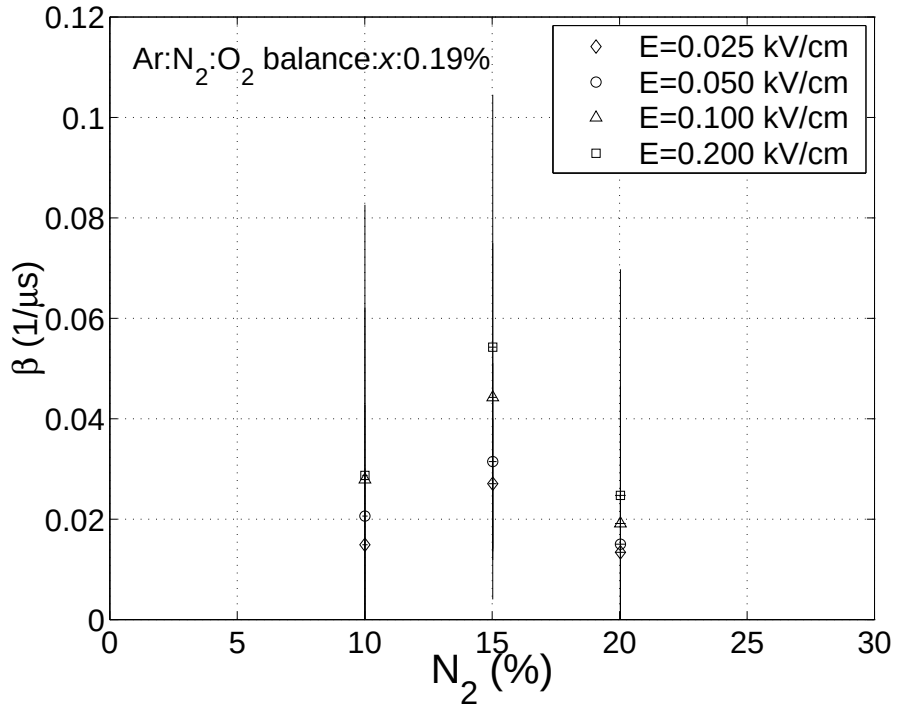

Figure 3-5: Mixtures with nitrogen but no carbon dioxide show much less attachment than mixtures with CO_2, and no trend of increasing attachment with nitrogen concentration.

When combined with carbon dioxide, however, nitrogen becomes an important contributor to attachment. Fig. 3-6 compares the dependence of attachment in a set of mixtures containing 5% N_2 to mixture with CO_2 alone (already shown in Fig. 3-3). The attachment rates produced by nitrogen and carbon dioxide together are

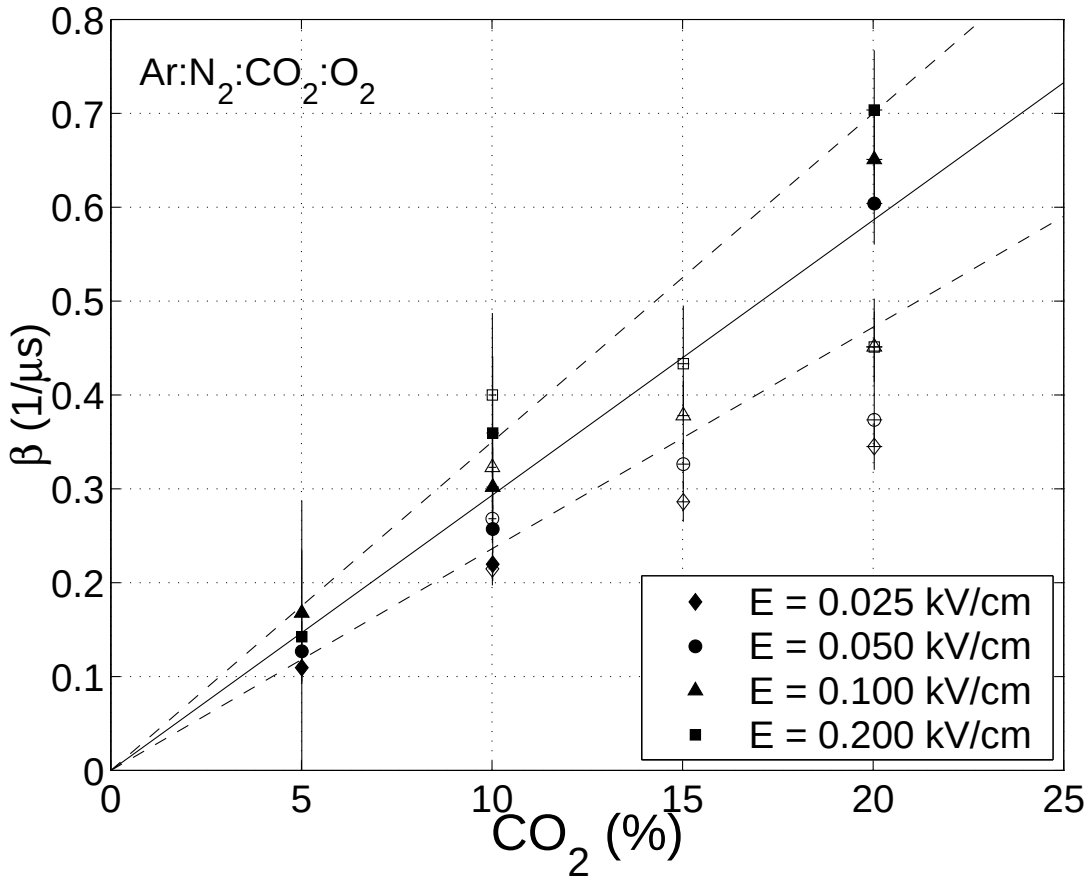

Figure 3-6: Adding 5% nitrogen alters attachment (β) in mixtures containing carbon dioxide. The filled points are nitrogen data; the unfilled points had no nitrogen. Oxygen was fixed at 1900 PPM and argon made up the balance of the mixtures. The solid line is the proportionality between β and CO_2 concentration in the nitrogen mixtures, with uncertainty indicated by the dashed lines.

not simple superpositions of their individual effects, indicating that the two interact, possibly through collisions with unstable states of oxygen. In the presence of 5% nitrogen, attachment rates become proportional to carbon dioxide concentration,

$$\beta\,(1/\mu\mathrm{s}) = ((1.5 \pm 0.4) \cdot 10^{-5})(\mathrm{PPM\,O_2})(\%\,\mathrm{CO_2}), \tag{3.8}$$

suggesting that the dominant attachment process is one in which CO_2 plays the stabilizing role of molecule X in Equation 3.2. The extrapolation indicates that there is no significant attachment in the absence of CO_2, in contrast with the measurements of mixtures without nitrogen.

This could be explained by nitrogen suppressing two-body attachment between electrons and oxygen molecules (increasing electron detachment from the oxygen molecules) while enhancing the probability of the three-body process with CO_2. These two effects would account for the low attachment in mixtures with only nitrogen and oxygen, and the switch to proportionality with carbon dioxide concentration in mixtures with both nitrogen and carbon dioxide. In support of the first effect, Herzenberg [9] states that the rate constant for attachment in nitrogen-oxygen mixtures is anomalously small, possibly due to electron detachment in collisions between N_2 and unstable oxygen molecules, O_2^{-*}.

Chapter 4

Summary

Attachment was not well described by simulations (see Fig 2-11, 2-12, 2-13), making empirical measurements essential to its study. Mixtures with abnormally large quantities of oxygen were measured to reduce experimental uncertainty, but attachment was found to be proportional to oxygen concentration, allowing extrapolation to attachment rates at normal drift chamber oxygen levels.

Equations 3.7, and 3.8 provide estimates of attachment in mixtures of argon and up to 20% carbon dioxide with and without 5% nitrogen. Attachment rates in mixtures with nitrogen and carbon dioxide are not superpositions of attachment rates in mixtures with the individual gases, indicating that N_2 and CO_2 interact in the attachment process.

Appendix A

Appendix: Initial chamber contamination

Before a measurement, the chamber is vacuumed for at least an hour. As it is vacuumed, air leaks into the chamber at $leak\,rate$=0.5 PSI/hr (see Section 2.2). So pressure in the chamber, p, as a function of time, t, is determined by

$$\frac{dp}{dt} = leak\,rate - vacuum\,rate. \tag{A.1}$$

To determine $vacuum\,rate$, a measurable pressure was placed in the chamber and evacuated. During evacuation, pressure as a function of time, $p(t)$, was recorded (Fig. A-1). One would expect the evacuation rate to be proportional to a pressure difference: The chamber pressure minus the vacuum pump's pressure, where the latter is assumed to be negligibly small.

$$\frac{dp}{dt} \approx -vacuum\,rate = -\frac{p}{t_v}, \tag{A.2}$$

so that the pressure decreases exponentially:

$$p = p_0 e^{-t/t_v}. \tag{A.3}$$

An exponential with time constant $t_v = 34 \pm 17$ s fits the data.

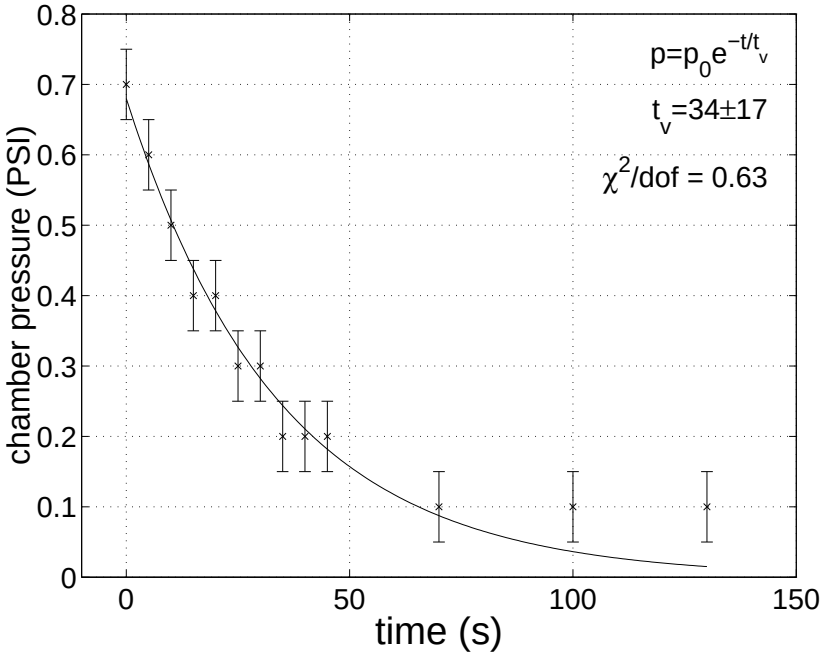

Figure A-1: Pressure was measured as the chamber was evacuated to determine t_v and *vacuum rate*.

At equilibrium after a long period of evacuation, $dp/dt = 0$ thus

$$leak\,rate = vacuum\,rate = \frac{p_{eq}}{t_v}, \tag{A.4}$$

$$p_{eq} = leak\,rate \cdot t_v = (5 \pm 2) \cdot 10^{-3}\,\text{PSI}. \tag{A.5}$$

At 0.03% of an atmosphere (300±150 PPM), this contamination does not significantly affect the partial pressures of argon, nitrogen, and carbon dioxide. It also small compared to the 800 PPM of oxygen contamination due to air leaking into the chamber during a measurement (see Section 2.2): Air is 20.9% oxygen, thus 60±30 PPM of oxygen contamination is present after vacuuming.

Bibliography

[1] U. Becker *et al.* MIT LNS Drift Gas R&D Home Page. *http://cyclotron.mit.edu/drift/*.

[2] U. Fano. *Annual Review of Nuclear Science*, volume 13, pages 1+. 1963.

[3] G. Charpak. Particle detection by means of gas discharges. *Journal de Physique I*, 30(5–6):11+, May 1969.

[4] W. Blum and L. Rolandi. *Particle Detection with Drift Chambers*, chapter 5.1, pages 155–158. Springer-Verlag, Heidelberg, Germany, 1993.

[5] G. Viertel *et al.* A time expansion chamber as a vertex detector. *Nuclear Instruments & Methods in Physics Research Section A*, A263(1):1–9, January 1988.

[6] E. Fortunato *et al.* Understanding the impact of additives with large inelastic cross sections on drift chamber performance. *Nuclear Instruments & Methods in Physics Research Section A*, 421(1–2):278–83, January 1999.

[7] U. Becker *et al.* Calibration setup for drift chamber gases. *Nuclear Instruments & Methods in Physics Research Section A*, 306(1–2):194–9, August 1991.

[8] S.F. Biagi. Monte Carlo simulation of electron drift and diffusion in counting gases under the influence of electric and magnetic fields. *Nuclear Instruments & Methods in Physics Research Section A*, 421(1–2):234–40, January 1999.

[9] A. Herzenberg. Attachment of slow electrons to oxygen molecules. *Journal of Chemical Physics*, 51(11):4942–4950, December 1969.

[10] Y. Kurihara *et al.* Cosmic ray tests of a 4.6 m-long test drift chamber for JLC. *Nuclear Instruments & Methods in Physics Research Section A*, 441(3):393–400, March 2000.